Optimized continuum from a photonic crystal fiber for broadband time-resolved coherent anti-Stokes Raman scattering

Young Jong Lee[1,2], Sapun H. Parekh[1], Yeon Ho Kim[1], and Marcus T. Cicerone[1,3]

[1]*Polymers Division, National Institute of Standards and Technology, Gaithersburg, MD 20899, USA*
[2]*yjlee@nist.gov*
[3]*cicerone@nist.gov*

Abstract: We demonstrate an optimization of continuum generation in a commercially available photonic crystal fiber and show that this continuum can be used to simultaneously measure vibrational dephasing times over an unprecedented frequency range of Raman modes. The dephasing time measurement is based on 2-pulse 3-color coherent anti-Stokes Raman scattering (CARS), and requires a continuum pulse that is coherent over a broad spectral bandwidth. We demonstrate that a continuum with the required characteristics can be generated from a photonic crystal fiber by appropriately conditioning the chirp of the excitation pulse and controlling its pulse energy. We are able to simultaneously measure vibrational dephasing times of multiple Raman modes (covering 500 cm^{-1} to 3100 cm^{-1}) of acetonitrile and benzonitrile using the optimized continuum with broadband time-resolved CARS.

2010 Optical Society of America

OCIS codes: (190.4370) Nonlinear optics, fibers; (300.6230) Spectroscopy, coherent anti-Stokes Raman scattering; (300.6500) Spectroscopy, time-resolved.

References and links

1. T. C. Bakker Schut, R. Wolthuis, P. J. Caspers, and G. J. Puppels, "Real-time tissue characterization on the basis of in vivo Raman spectra," J. Raman Spectrosc. **33**(7), 580–585 (2002).
2. T. W. Kee, and M. T. Cicerone, "Simple approach to one-laser, broadband coherent anti-Stokes Raman scattering microscopy," Opt. Lett. **29**(23), 2701–2703 (2004).
3. H. Kano, and H. Hamaguchi, "Femtosecond coherent anti-Stokes Raman scattering spectroscopy using supercontinuum generated from a photonic crystal fiber," Appl. Phys. Lett. **85**(19), 4298–4300 (2004).
4. Y. J. Lee, Y. Liu, and M. T. Cicerone, "Characterization of three-color CARS in a two-pulse broadband CARS spectrum," Opt. Lett. **32**(22), 3370–3372 (2007).
5. Y. J. Lee, and M. T. Cicerone, "Vibrational dephasing time imaging by time-resolved broadband coherent anti-Stokes Raman scattering microscopy," Appl. Phys. Lett. **92**(4), 041108 (2008).
6. A. Laubereau, and W. Kaiser, "Vibrational Dynamics of Liquids and Solids Investigated by Picosecond Light-Pulses," Rev. Mod. Phys. **50**(3), 607–665 (1978).
7. A. Morresi, L. Mariani, M. R. Distefano, and M. G. Giorgini, "Vibrational-Relaxation Processes in Isotropic Molecular Liquids - A Critical Comparison," J. Raman Spectrosc. **26**(3), 179–216 (1995).
8. H. Kano, and H. Hamaguchi, "Dispersion-compensated supercontinuum generation for ultrabroadband multiplex coherent anti-Stokes Raman scattering spectroscopy," J. Raman Spectrosc. **37**(1-3), 411–415 (2006).
9. D. Pestov, R. K. Murawski, G. O. Ariunbold, X. Wang, M. C. Zhi, A. V. Sokolov, V. A. Sautenkov, Y. V. Rostovtsev, A. Dogariu, Y. Huang, and M. O. Scully, "Optimizing the laser-pulse configuration for coherent Raman spectroscopy," Science **316**(5822), 265–268 (2007).
10. B. von Vacano, and M. Motzkus, "Time-resolving molecular vibration for microanalytics: single laser beam nonlinear Raman spectroscopy in simulation and experiment," Phys. Chem. Chem. Phys. **10**(5), 681–691 (2008).
11. A. Volkmer, L. D. Book, and X. S. Xie, "Time-resolved coherent anti-Stokes Raman scattering microscopy: Imaging based on Raman free induction decay," Appl. Phys. Lett. **80**(9), 1505–1507 (2002).
12. J. P. Ogilvie, E. Beaurepaire, A. Alexandrou, and M. Joffre, "Fourier-transform coherent anti-Stokes Raman scattering microscopy," Opt. Lett. **31**(4), 480–482 (2006).
13. K. B. Shi, P. Li, and Z. W. Liu, "Broadband coherent anti-Stokes Raman scattering spectroscopy in supercontinuum optical trap," Appl. Phys. Lett. **90**(14), 141116 (2007).
14. J. M. Dudley, G. Genty, and S. Coen, "Supercontinuum generation in photonic crystal fiber," Rev. Mod. Phys. **78**(4), 1135–1184 (2006).

15. B. Schenkel, R. Paschotta, and U. Keller, "Pulse compression with supercontinuum generation in microstructure fibers," J. Opt. Soc. Am. B **22**(3), 687–693 (2005).
16. M. A. Foster, A. L. Gaeta, Q. Cao, and R. Trebino, "Soliton-effect compression of supercontinuum to few-cycle durations in photonic nanowires," Opt. Express **13**(18), 6848–6855 (2005).
17. N. Nishizawa, and J. Takayanagi, "Octave spanning high-quality supercontinuum generation in all-fiber system," J. Opt. Soc. Am. B **24**(8), 1786–1792 (2007).
18. L. B. Fu, B. K. Thomas, and L. Dong, "Efficient supercontinuum generations in silica suspended core fibers," Opt. Express **16**(24), 19629–19642 (2008).
19. Certain equipment is identified in this Letter to specify adequately the experimental details. Such identification does not imply recommendation by the National Institute of Standards and Technology, nor does it imply that the equipment is necessarily the best available for this purpose.
20. http://nktphotonics.com/files/files/datasheet_fw-800.pdf
21. J. M. Dudley, and S. Coen, "Numerical simulations and coherence properties of supercontinuum generation in photonic crystal and tapered optical fibers," IEEE J. Sel. Top. Quantum Electron. **8**(3), 651–659 (2002).
22. J. B. Guild, C. Xu, and W. W. Webb, "Measurement of group delay dispersion of high numerical aperture objective lenses using two-photon excited fluorescence," Appl. Opt. **36**(1), 397–401 (1997).
23. H. W. Hubble, T. S. Lai, and M. A. Berg, "Raman free-induction-decay measurements in low viscosity and supercooled toluene: Vibrational dephasing by shear fluctuations," J. Chem. Phys. **114**(8), 3662–3673 (2001).
24. R. Inaba, H. Okamoto, K. Yoshihara, and M. Tasumi, "Observation of the dephasing of the C.tplbond.N stretching vibration in liquid nitriles by femtosecond time-resolved coherent anti-Stokes Raman scattering," J. Phys. Chem. **96**(21), 8385–8390 (1992).
25. D. Vanden Bout, L. Muller, and M. Berg, "Ultrafast Raman echoes in liquid acetonitrile," Phys. Rev. Lett. **67**(26), 3700–3703 (1991).
26. M. Fickenscher, and A. Laubereau, "High-Precision Femtosecond CARS of Simple Liquids," J. Raman Spectrosc. **21**(12), 857–861 (1990).
27. R. Inaba, K. Tominaga, M. Tasumi, K. A. Nelson, and K. Yoshihara, "Observation of Homogeneous Vibrational Dephasing in Benzonitrile by Ultrafast Raman Echoes," Chem. Phys. Lett. **211**(2-3), 183–188 (1993).
28. H. Okamoto, R. Inaba, K. Yoshihara, and M. Tasumi, "Femtosecond Time-Resolved Polarized Coherent Anti-Stokes Raman Studies on Reorientational Relaxation in Benzonitrile," Chem. Phys. Lett. **202**(1-2), 161–166 (1993).
29. H. Hamaguchi, and T. L. Gustafson, "Ultrafast Time-Resolved Spontaneous and Coherent Raman-Spectroscopy - the Structure and Dynamics of Photogenerated Transient Species," Annu. Rev. Phys. Chem. **45**(1), 593–622 (1994).
30. J. C. Deäk, L. K. Iwaki, and D. D. Dlott, "Vibrational energy redistribution in polyatomic liquids: Ultrafast IR-Raman spectroscopy of acetonitrile," J. Phys. Chem. A **102**(42), 8193–8201 (1998).
31. D. Bhattacharjee, A. G. (Purkayastha), T. N. Misra, and S. K. Nandy, "Raman Spectral Study of Vibrational Relaxation of the CN Stretching Band of Acetonitrile and Benzonitrile," Journal of Raman Spectroscopy **27**(6), 457–461 (1996).
32. B. Dick, "Response Function-Theory of Time-Resolved CARS and CSRS of Rotating Molecules in Liquids Under General Polarization Conditions," Chem. Phys. **113**(1), 131–147 (1987).

1. Introduction

Subtle chemical changes in biological and materials systems associated with changes of state can be detected using Raman spectroscopy [1]. Broadband coherent anti-Stokes Raman scattering (CARS) microscopy can provide both coherently enhanced signal and broad spectral bandwidth ($\sim$3000 cm^{-1}) needed to detect such changes in crowded Raman spectra in both the fingerprint and CH stretch regions from complex biological and materials samples [2,3]. A 2-pulse broadband CARS signal can be generated by overlapping a narrowband and a continuum pulse via two mechanisms [4]. In the "2-color" CARS mechanism, the pump and probe transitions are degenerately induced by the narrowband pulse, and the Stokes transition by the continuum pulse. In the "3-color" CARS mechanism, two different frequency components in the continuum pulse induce the pump and Stokes transitions and the narrowband pulse induces the probe transition. Unlike 2-color CARS, 3-color CARS can be used to measure the dynamics of vibrationally excited states by controlling the time delay between the continuum and narrowband pulses. In this way, the 2-pulse 3-color microscopy approach can provide vibrational dephasing time images [5], which are a potential imaging modality of the local molecular environment of vibrational modes. In addition, the time-delay control allows separation of nonresonant background (NRB) contribution from the resonant signal by taking advantage of different time scales of NRB (<10 fs) and resonant vibrational coherence (0.5 ps $\sim$10 ps) [6,7]. Various types of time-resolved approaches have been used for NRB-free CARS spectroscopy [8–10] and microscopy [5,11–13]. Recently, a 3-color 3-pulse time-resolved scheme has been coupled with multiplex CARS techniques to acquire NRB-free

spectra with a high spectral resolution and a relatively broad spectral range (~900 cm^{-1}) [9]. However, such approaches require elaborate laser systems, including a kilohertz repetition rate amplifier and an additional optical parametric amplifier. Another approach is to Fourier-transform time-domain CARS signals acquired at scanned time delays between two well compressed femtosecond pulses [10,12]. With these methods, the upper limit of the measurable frequency is determined by the pulse width of the compressed pulse, demonstrated up to ~1300 cm^{-1}. To our knowledge, the only way that has been demonstrated to achieve a 2000 cm^{-1} or greater Raman frequency range from an unamplified and high repetition-rate source is to use continuum from a highly nonlinear fiber [2,3]. However, in 2-pulse 3-color CARS, based on continuum generation in such fibers, the spectral range and signal intensity can be limited by large nonlinear dispersion and soliton splitting in the continuum pulse despite its broad bandwidth [4]. The ideal continuum pulse for 3-color CARS imaging should be (i) maximally coherent (i.e., transform-limited), (ii) sufficiently broad in frequency (>3500 cm^{-1} on the long wavelength side of the narrowband pulse), and (iii) sufficiently powerful (>10 mW at the sample position for 80 MHz repetition rate). Similar criteria exist for any application that involves use of continuum light for intrapulse multiphoton excitation. Extensive theoretical and experimental studies have been performed to control the characteristics of continuum pulses by varying the parameters of both the medium (fiber length, nonlinearity, dispersion curve) and the input pulse (wavelength, pulsewidth, pulse energy, polarization, and chirping) [14]. Previous reports have shown continuum generation from nonlinear fibers with ultrashort (<10 fs) pulse widths [15,16] and octave-spanning bandwidths [17,18]. However it remains extremely challenging to generate a continuum pulse that simultaneously satisfies the three requirements of coherence, bandwidth, and power. We present an experimental optimization of continuum generation in a commercially available fiber that produces a sufficiently broad, coherent, and energetic pulse to generate a strong 3-color CARS signal with unprecedented bandwidth. We vary power and dispersion of the excitation pulse in order to maximize continuum pulse bandwidth, minimize soliton splitting, and maintain sufficiently high output pulse energy to generate a robust 3-color CARS microscopy signal. The intuitive explanation of our results, based on extant literature, suggests a path forward for further improving the characteristics of the continuum pulse for the 3-color CARS application.
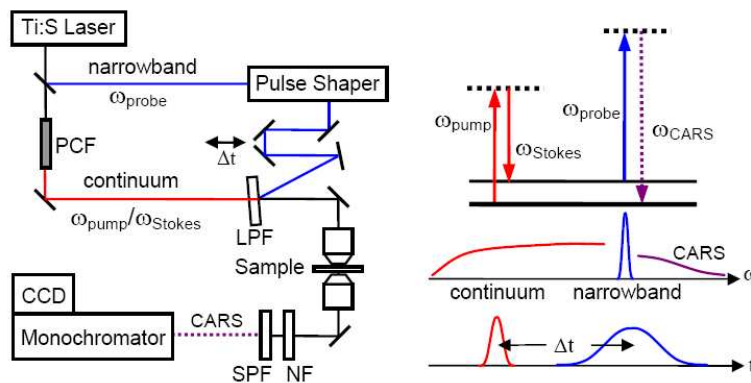
Fig. 1. Experimental scheme and energy diagram of the 2-pulse broadband CARS setup for vibrational dephasing time measurement: PCF, photonic crystal fiber; LPF, longpass filter; NF, notch filter; SPF, shortpass filter.

2. Experimental setup

The experimental setup of the 2-pulse time-resolved broadband CARS microscope (Fig. 1) is similar to our previous configurations [5]. Briefly, the output of a Ti:sapphire laser oscillator (MaiTai, Spectra Physics) [19] centered at 830 nm with a transform-limited pulse width of 70

fs and 80 MHz repetition rate was sent through a pre-compensation unit (DeepSee, Spectra Physics) to adjust the group delay dispersion (GDD) of the output from −4000 fs^2 to −21000 fs^2 without changing its average power and spectrum. The output pulse was split into two parts. One part was used to generate a continuum from a 12 cm photonic crystal fiber (Femtowhite800, Crystal Fibre). The remaining oscillator output was introduced into a 4*f*-pulse shaper with a spatial light modulator (SLM-640-D-NM, CRI). The pulse shaper was used to adjust the bandwidth of the narrowband pulse and to make the narrowband pulse transform-limited at the sample position. The two beams were combined by an 850 nm longpass filter (Omega Filters) and collinearly introduced with parallel linear polarization into a 40X, 0.95 NA objective lens (Olympus). The CARS signal was collected in the forward direction and passed through a notch filter and a shortpass filter. The spectrum of the filtered CARS signal was analyzed with a CCD (DU920N-BR-DD, Andor) attached to a monochromator (SP-2300i, Acton).
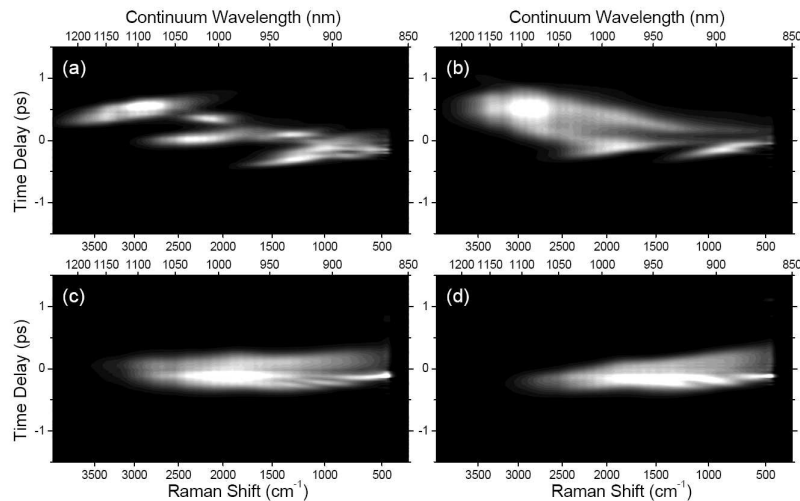
Fig. 2. Time-resolved CARS spectra generated in a glass coverslip. The continuum pulse is generated from a photonic crystal fiber pumped by a pulse with different group delay dispersion (GDD) of (a) −4000 fs^2, (b) −12000 fs^2, (c) −18000 fs^2, and (d) −21000 fs^2, where the uncertainty of GDD is 500 fs^2. For each spectrum the phase of the narrowband pulse is optimized to the transform limit at the sample position. The continuum-generating pulse is centered at 830 nm and its average power is 350 mW before the fiber. Average powers of the continuum and narrowband pulses are 2 mW and 24 mW, respectively at the sample position. The exposure time was 100 ms.

3. Results and discussion

Figures 2 and 3 show time-resolved nonresonant CARS spectra from a glass coverslip. Because of the low continuum power used to generate these spectra, they are dominated by 2-color signal, and thus their time-evolution mirrors the temporal profile of the continuum pulse. We use these as a diagnostic to highlight the influence of input pulse dispersion and power on the continuum bandwidth and temporal profile. Controlled parameters of the input pulse include wavelength, dispersion, and power. Input pulse wavelengths tested for continuum generation are 765 nm, 830 nm, and 860 nm, all of which are in the anomalous region of the fiber dispersion curve [20]. The long wavelength end of the generated continuum spectrum is not sensitive to the input pulse wavelength and remains ~1200 nm at an average input power of 350 mW (4.4 nJ/pulse). The short wavelength end of the continuum at the sample position is determined by the cutoff wavelength of the longpass filter combining the continuum and narrowband beams, and the lower limit of the filter cutoff wavelength is determined by the probe wavelength. We used an 830 nm narrowband pulse and an 850 nm longpass filter for the data acquisition reported in the remainder of this report. In Fig. 2, we show continuum

time profiles with different amounts of negative GDD applied to the input pulse, each with the same average power. We observe that an input pulse with a small, negative GDD generates a somewhat unstable continuum with broad bandwidth, but also multiple solitons having significant temporal separation [Fig. 2(a)]. As the input pulse becomes more negatively chirped, the soliton splitting is greatly mitigated and the pulse becomes more stable, but as the magnitude of the negative GDD increases further, [Fig. 2(d)] the bandwidth begins to narrow. The weakening of soliton splitting may be related with the negative dispersion itself or simply to reduced peak power due to pulse broadening [14]. The 70 fs transform-limited pulse will be temporally broadened to 170 fs and 800 fs by GDD of -4000 fs^2 and -21000 fs^2, respectively. We are interested in the most stable continuum with the broadest bandwidth and least chirp for 3-color CARS generation.
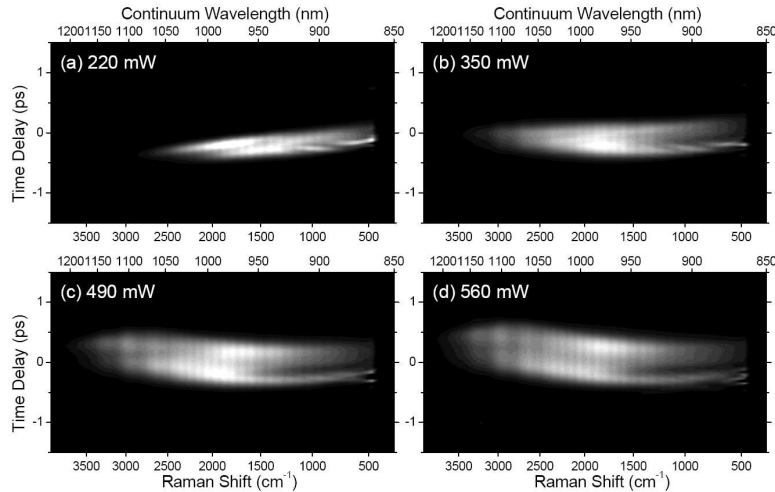
Fig. 3. Time-resolved CARS spectra generated in a glass coverslip by continuum pulses generated by a input pulse with different average powers of (a) 220 mW, (b) 350 mW, (c) 490 mW, and (d) 560 mW. At the sample position, the average powers of the continuum and narrowband pulses were controlled at constant values of 2 mW and 25 mW, respectively. The exposure time was 100 ms. The GDD of the input pulse is -19000 fs^2.

We can also use input pulse power to optimize the continuum. Increasing input pulse power increases the bandwidth of the continuum until, at an input power of 350 mW, the long wavelength end reaches 1200 nm. Beyond this "saturation" input power, additional power only leads to more complex structure in the time domain [Figs. 3(c) and 3(d)] and results in less efficient CARS generation. Theoretical and numerical studies have shown that the majority of spectral broadening occurs within the initial stages of propagation. The length of the initial stage depends on various parameters of laser and fiber, including laser power. For a fixed fiber length, higher peak power will cause the initial broadening to occur earlier, imparting greater fiber-induced dispersion to the output continuum, and eventually lead to soliton splitting [21]. This scenario is consistent with the data of Fig. 2 as well as Fig. 3. At a higher power [Figs. 3(c) and 3(d)] the average GDD of the continuum is -200 fs^2, while that by a lower power [Fig. 3(a)] is $+500$ fs^2. From the average dispersion of the fiber (~70 ps/(km·nm) [20]) in the continuum wavelength range, we can equate this difference in chirp of output continuum to a difference in the propagation within in the fiber of ~2 cm; at higher power, the pulse seems to be generated ~2 cm earlier than at low power. Thus, by tuning both chirp and power of the input pulse, we have some control over the continuum chirp, and we can pre-compensate for the dispersion of an objective lens, yielding a mean continuum GDD of near-zero at the sample position. The GDD of a continuum output can be varied to a value as large as 4500 fs^2, depending on where the continuum broadening occurs in the 12 cm fiber while the GDD of typical high numerical aperture objective lenses are 2000 fs^2 ~6500 fs^2 [22].

This fortuitous GDD cancellation removes necessity of additional pulse compression or pulse shaping for the continuum pulse, allowing maximum power delivery for the continuum pulse into the sample position even though the higher order dispersion is still not compensated.
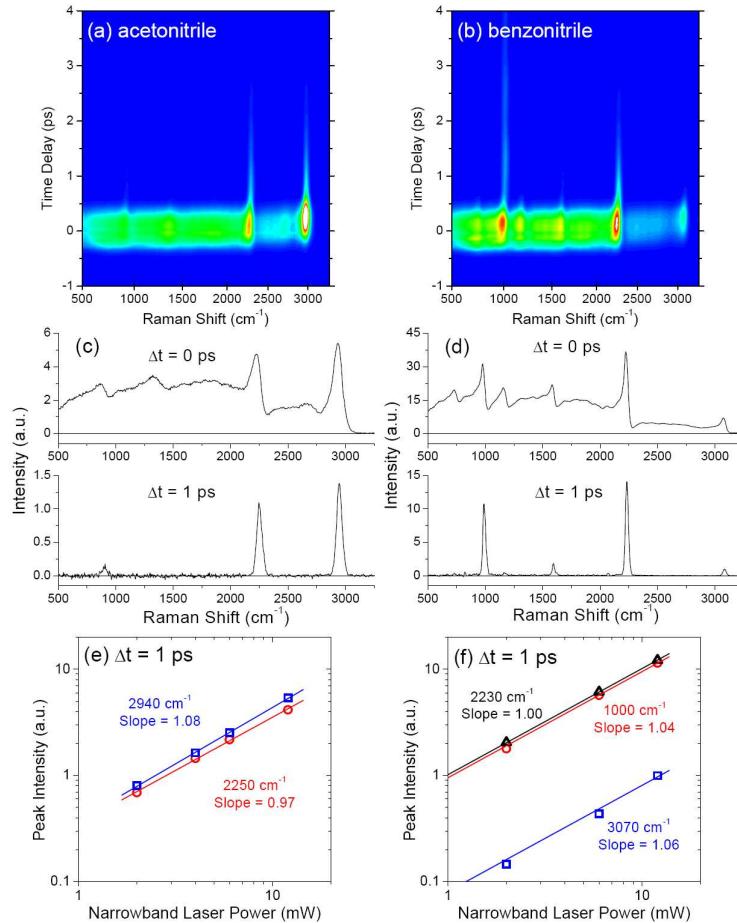
Fig. 4. Time-resolved CARS spectroscopy of neat (a) acetonitrile and (b) benzonitrile. CARS spectra at $\Delta t = 0$ and 1 ps are shown for (c) acetonitrile and (d) benzonitrile. Peak intensities at time delay, $\Delta t = 1$ ps, are plotted as a function of narrowband pulse power at the sample position for (e) acetonitrile and (f) benzonitrile. Log-log plots of the peak intensities at $\Delta t = 1$ ps are fitted to $\log(I) =$ slope*$\log(P)$ + constant, where I is the intensity, P is the average power of the narrowband pulse. The fitted slopes are all close to unity, confirming that the signal at $\Delta t = 1$ ps is generated by the 3-color CARS mechanism. The average power of the continuum pulse was constant at 14 mW, and the average power of the narrowband pulse was 1 mW at the sample position for (a)-(d). For each time scan, the time-independent baseline was measured at $\Delta t = -2$ ps and subtracted from the total CARS spectrum data. The baseline was (10 to 20) % of the peak signal. The exposure time was 600 ms.

Based on needs for generation of 3-color CARS, an appropriate amount of power and GDD of the excitation pulse should be chosen for both a reasonable Raman shift range and signal intensity. For the remainder of this study, an input pulse power of 350 mW and the GDD of -19000 fs^2 are used to generate the continuum pulse for broad and strong 3-color CARS generation. The input pulse polarization is matched to the polarization axis of the fiber, which provides the highest throughput and polarization extinction of the output continuum, which will maximize the efficiency of CARS signal generation. The output power of the continuum is measured as 40 mW after the 850 nm longpass filter and the power is reduced with a neutral density filter to an appropriate level at the sample position. It should be noted

that one may achieve a continuum with similar bandwidth, but possibly a greater degree of coherence using different length or different dispersion of fiber.
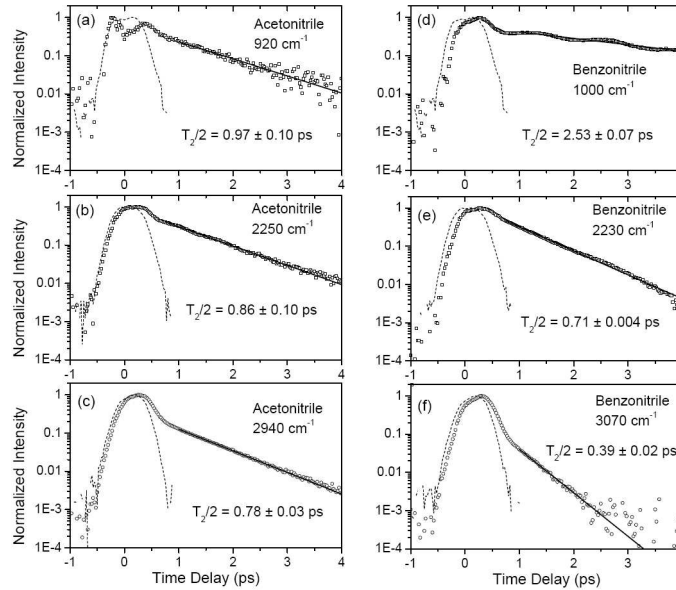
Fig. 5. Dephasing time measurements of various Raman modes of neat (a-c) acetonitrile and (d-f) benzonitrile. The dotted lines indicate time profiles of the nonresonant background signal from a glass coverslip at the same Raman shift in each figure. The data of time delay (Δt) later than 1 ps are fitted to a single exponential function, $I(t) = \exp(-2\Delta t/T_2)$, where T_2 is the vibrational dephasing time. The average powers of the continuum and narrowband pulses were 14 mW and 1 mW, respectively, at the sample position. The exposure time was 600 ms.

Figure 4 shows time resolved CARS results from neat acetonitrile and benzonitrile using the optimized continuum pulse in the 3-color arrangement. The time resolved data show clear differences in the measured CARS spectra of $\Delta t = 0$ ps and 1 ps. At $\Delta t = 0$ ps, NRB of both 2- and 3-color CARS interferes with resonant signal and produces dispersive line shapes overlaid on a broad baseline. At $\Delta t = 1$ ps, the NRB contribution diminishes and only 3-color resonant CARS signal remains. The log-log plots of the peak height at $\Delta t = 1$ ps in Figs. 4(e) and 4(f) show a linear dependence on the narrowband pulse power, which confirms that the time-delayed spectra are generated by the 3-color CARS mechanism. The frequency range shown in the time-resolved spectra is noteworthy - in previously reported NRB-free CARS spectra using similar time-resolved techniques, Raman peaks are barely analyzable at frequencies greater than 2300 cm^{-1} [5]. This higher-frequency region includes CH stretch resonances, whose dephasing time will be impacted by biologically important phenomena, such as membrane phase changes. The optimized time-resolved broadband CARS technique presented here provides access to vibrational dephasing times of multiple Raman modes from 500 cm^{-1} to 3100 cm^{-1} in a single time delay scan without any additional laser tuning. This broad frequency range is not available in the conventional non-collinear coherent time-resolved techniques in a bulk sample due to the strict phase matching condition. Figure 5 shows time evolution of low, medium, and high frequency Raman modes, extracted from the data shown in Figs. 4(a) and 4(b). The bandwidth of the narrowband pulse can be easily adjusted to give the desired temporal and spectral resolution considering the dephasing time of a mode and its frequency proximity to adjacent Raman modes. For Figs. 4 and 5, the narrowband pulse is shaped to a Gaussian function with the full-width-half-maximum (FWHM) of 50 cm^{-1}, which corresponds to 300 fs in the time domain. For the instrumental response functions (IRF), the time profiles are measured from a glass cover slip (a nonresonant medium) under the same measurement condition as the sample liquids, and the IRF FWHM ranges between 500 fs and

550 fs (the dotted lines in Fig. 5). Data only after $\Delta t > 1$ ps are used for analysis to avoid the interference from NRB contribution when the pulses overlap. The time profiles are fitted to single exponential functions, $I(\Delta t) = \exp(-2\Delta t/T_2)$, where T_2 is the vibrational dephasing time [7].

The fitted values of $T_2/2$ for acetonitrile and benzonitrile are summarized in Table 1. The values for the CC stretch mode (920 cm^{-1}), the CN stretch mode (2250 cm^{-1}), and the CH stretch mode (2940 cm^{-1}) agree reasonably well with literature values from other time-resolved methods. For benzonitrile we obtain $T_2/2$ values for the ring breathing mode (1000 cm^{-1}), the CN stretch mode (2230 cm^{-1}), and the CH stretch mode (3070 cm^{-1}). Here as well, the CN stretch mode results agree well with previously reported values. A $T_2/2$ value for the CH stretch mode has not been reported in benzonitrile, but for comparison, the $T_2/2$ value of the CH stretch mode in polystyrene measured by 3-pulse time-resolved CARS is 0.39 ps [11], which agrees well with our measured value. The time profile of the ring breathing mode exhibits quantum beating due to coherent excitation of adjacent vibrational excited states, which have been observed in previous femtosecond time-resolved CARS measurements [5,23], where the reported $T_2/2$ values are also close to the values found here.

Table 1. Summary of $T_2/2$ values measured in this study and comparison with previously reported values

Sample	Raman mode	Frequency (cm^{-1})	$T_2/2$ (ps)	
			This report	Previous reports
acetonitrile	CC stretch	920	0.97 ± 0.10[a]	
	CN stretch	2250	0.86 ± 0.02	0.87 [24]
	CH stretch	2940	0.78 ± 0.03	0.8 [25]; 0.86 [26]
benzonitrile	Ring breathing	1000	2.53 ± 0.07	2.7 [5]; 2.93[b] [23]
	CN stretch	2230	0.71 ± 0.004	0.6 [27]; 0.76 [28]
	CH stretch	3070	0.39 ± 0.02	0.39[c] [11]

[a]The uncertainty indicates the standard deviation of fitted values from six separate measurements.
[b]Measured in toluene.
[c]Measured in polystyrene.

It should be noted that the time profile measured by this 2-pulse time-resolved CARS technique contains not only the vibrational dephasing process but other dynamic processes, including vibrational depopulation and rotational motion [7]. The vibrational depopulation time, T_1, can cause the measured dephasing time, T_2, to be shorter than the pure dephasing time, T_2^*, as $1/T_2 = 1/(2T_1) + 1/T_2^*$. For most liquids and solutions at room temperature, T_1 is considerably longer than T_2 and the perturbation of T_2 by T_1 is negligible [6,29]. For example, the T_1 values of liquid acetonitrile are 45 ps, 80 ps, and 5 ps for the CC stretch, CN stretch, and CH stretch modes, respectively [30]. Similarly, rotational motion of molecules can affect the time profile of CARS signals when the anisotropy tensor element (or the depolarization ratio) of a Raman mode is large and the time scale of rotation is comparable to T_2. However, in many practical cases, the values of anisotropy tensor elements are small and the rotation times and T_2 are sufficiently dissimilar that contribution of molecular rotation may be negligible [6]. For example, the depolarization ratio of the CN stretch modes are 0.04 and 0.045 for acetonitrile and benzonitrile, respectively [31], and the reorientational relaxation time is 5.58 ps for the CN mode of neat benzonitrile [28]. To minimize the rotational motion contribution experimentally, the magic angle polarization configuration can be applied [32] by using a set of accurately adjusted waveplates, but complete suppression of the contribution may still be difficult to achieve due to polarization mixing associated with tight focusing at the sample position.

4. Conclusion

Continuum generation from a commercially available canisterized fiber has been optimized for 2-pulse broadband time-resolved CARS spectroscopy to measure a 3-color CARS spectrum with a wide frequency range from 500 cm^{-1} to >3100 cm^{-1} in a single measurement without any additional laser tuning. We demonstrate this by measuring vibrational dephasing times of several Raman modes of two liquids; the values we obtain for dephasing times agree well with previously reported values measured by single-frequency time-resolved methods. Additionally, as shown in the previous papers [5], this time-resolved CARS technique is based on a nonlinear imaging system so that it can be used to measure correlation between the spatial morphology and the molecular dynamics of heterogeneous samples.